Sensitive and simultaneous detection of different pathogens by surface-enhanced Raman scattering based on aptamer and Raman reporter co-mediated gold tags

Yuzhi Li[a,b], Chang Lu[a], Shuaishuai Zhou[a], Marie-Laure Fauconnier[b], Fei Gao[a], Bei Fan[a], Jianhan Lin[c], Fengzhong Wang[a], and Jinkai Zheng[a,*]

[a] Institute of Food Science and Technology, Chinese Academy of Agricultural Sciences, Beijing 100193, P. R. China

[b] Laboratory of Chemistry of Natural Molecules, Gembloux Agro-Bio Tech, University of Liege, Gembloux 5030, Belgium

[c] Key Laboratory of Agricultural Information Acquisition Technology, Ministry of Agriculture and Rural Affairs, China Agricultural University, Beijing, 100083, China

* Corresponding author: Jinkai Zheng, Tel: (086)-010-62819501, Fax: (086)-010-62819501.

E-mail address: zhengjinkai@caas.cn (J. Zheng).

ABSTRACT

A biosensor based on novel SERS tags, consisting of gold nanorods (GNRs) complexed with oligonucleotide aptamers and the Raman reporters, was developed for the sensitive and simultaneous detection of different food pathogens. The aptamers not only act as bio-recognition molecules, but along with the Raman reporters, induce the GNRs to grow to specific shapes, which in turn enhance the Raman signal and facilitate sensitive detection. Signal interference during the simultaneous detection of pathogens is avoided, due to the stable anchored aptamers and embedded Raman reporters. We combined the novel SERS tags with antibody-modified magnetic nanoparticles to create a biosensor capable of simultaneous detection of *E. coli* O157:H7 and *S. typhimurium* with good linear response (10^1 to 10^6 cfu/mL), high detection sensitivity (< 8 cfu/mL) and recovery rate (95.26%-107.88%) in spiked food samples. This strategy achieves the goal of sensitive and simultaneous quantitative detection of pathogens.

Keywords: surface enhanced Raman scattering (SERS); pathogens; simultaneous; aptamer; biosensor.

1 Introduction

Foodborne pathogens are a global public health issue. *Escherichia coli* O157:H7 and *Salmonella typhimurium* are the most commonly reported foodborne pathogens. They cause serious issues such as bloody diarrhea [1,2], intestinal infectious diseases [3], food poisoning [4], and even death. Simultaneous detection of multiple foodborne pathogens is of the utmost importance to offer more useful information for illness control, in comparison to single species pathogen, due to the multiple contaminations. Currently, the screening and detection pathogen is mainly done by culture plate [5], polymerase chain reaction [6], enzyme-linked immunosorbent assay [7], or by biosensors based on electrochemistry [8], quartz crystal microbalance [9], or surface plasmon resonance methods [10]. However, the sensitive and simultaneous detection of multiple foodborne pathogens is still restricted by signal interference, lack of sufficient sensitivity, or difficulty achieving quantitative detection, which is important information for early screening and disease control.

Surface-enhanced Raman scattering (SERS) is an ultrasensitive, vibrational spectroscopic technique that enables the detection of molecules on or near the surface of a noble metal nanostructure, which, due to local surface plasmon resonance, greatly enhances the strength of the Raman signal [5]. SERS-based biosensors, possessing fingerprint precision, high sensitivity and quantitative detection capability [11], have been widely used for pathogen detection. Label –based SERS method has higher sensitivity than label-free method attributed to the specific binding of the aptamers, leading to sharp characteristic peaks in the spectra of the Raman reporters, and to the strong and stable enhancement of the noble metal substrates [12-14]. However, existing SERS tags used for the simultaneous detection of pathogens are generally prepared by adsorbing Raman reporters onto the surface of nanomaterials, which are easily

eliminated and destroyed during subsequent washing treatments [15]. The limited surface area of nanomaterials also affects the adsorption of Raman reporters onto their surfaces [16].

To solve these problems, SERS tags containing core-shell structures have been developed to improve the stability, as well as the signal reproducibility, of the tags [17]. A variety of coating materials have been applied to the surface of SERS tags to create these core-shell structures [18-20]. Once the basic core-shell structure is established, chemical or biological groups modified molecules may be subsequently added [21-23]. The core-shell SERS tags-based method can provide a relatively stable and reproducible SERS signal, but the complicated syntheses and high cost limit its application. There is a need for simple fabrication methods for SERS tags, possessing stable and strong Raman signals and specific bio-recognition to realize the simultaneous detection of foodborne pathogens [24-27].

DNA binds to gold via surface-binding moieties such as carbonyls and amides, with an adsorption ability order of G> A> C> T [28]. Meanwhile, the morphology of nanomaterials can be regulated by DNA to form nanoparticles and nanorods with specific sharp shapes [29,30]. According to the electromagnetic field enhancement principle, a sharp morphology produces a "hotspot" effect to facilitate Raman signal enhancement [31]. Furthermore, during the regrowth of the nanostructures, DNA molecules not only provide a stable anchor in the outer layer of the nanomaterial, but also retain their bio-recognition properties [32], providing an opportunity for aptamer-sequence design and multipurpose usage in SERS tag fabrication. However, producing embedded reporter and DNA-based SERS tags directly and controllably with stable and strong Raman signals is difficult. Our team has recently developed nanobones shaped SERS tags for the detection of *E. coli* O157:H7 [33], while more challenging work is developing a multiplex biosensor capable of recognizing multiple pathogens simultaneously, which could overcome the

limitations of signal interference and sensitivity.

To realize the sensitive and simultaneous detection of *E. coli* O157:H7 and *S. typhimurium*, we have developed a novel biosensor based on different morphologically controllable SERS tags via Raman reporter and aptamer co-mediated gold nanorods (GNRs). The tags, grown using one-pot synthesis, provide stable and strong characteristic signals, as well as bio-recognition specificity, thus avoiding signal interference during the simultaneous detection of pathogens. SERS tags with cracked octahedral shapes and small protrusion morphologies were fabricated using two different Raman reporters and specifically designed aptamers during mediated regrowth of the GNRs. Assisted by antibodies conjugated onto modified magnetic nanoparticles, *E. coli* and *S. typhimurium* were simultaneously and quantitatively detected within 10^1–10^6 cfu/mL with LODs of 5 and 8 cfu/mL, respectively. This biosensor, benefiting from the novel SERS tags, realizes the goal of sensitive and simultaneous quantitative detection of bacteria, and may possibly become a universal detection tool for the daily simultaneous detection of foodborne pathogens.

2 Materials and methods

2.1 Chemical and biochemical materials

Chloroauric acid trihydrate ($HAuCl_4$), cetyltrimethylammonium bromide (CTAB), sodium borohydride, ascorbic acid, silver nitrate, DTNB, MBA, bovine serum albumin (BSA), hydroxylamine hydrochloride (HA), and sodium hydroxide were purchased from Sigma-Aldrich (St. Louis, MO, USA). Streptavidin-modified magnetic nanoparticles (MNPs) of 150 nm diameter were obtained from Ocean nanotech (Dunedin, FL, USA). The Luria–Bertani medium (LB), alkaline peptone water medium, and agar were purchased from Aoboxing Biotech (Beijing,

China). Phosphate-buffered saline (PBS), *E. coli* O157:H7 (ATCC 43888), *S. typhimurium* (ATCC14028), *E. coli* (ATCC 25922), *Vibrio parahemolyticus* (ATCC 17802), and *S. aureus* (ATCC 25923) were purchased from Solarbio Life Sciences (Beijing, China). Rabbit antibody against *E. coli* O157:H7, and mouse antibody against *S. typhimurium*, were purchased from Meridian Life Science (Memphis, TN, USA). A Long-Arm Biotin Labeling Kit from Elabscience Biotechnology (Wuhan, China) was used for the modification of antibodies. The designed aptamers for *E. coli* O157:H7 (TTTTT TTTTT TTTTT TTTTT CCGGA CGCTT ATGCC TTGCC ATCTA CAGAG CAGGT GTGAC GG) [34] and *S. typhimurium* (CCCCC CCCCC CCCCC CCCCC TATGG CGGCG TCACC CGACG GGGAC TTGAC ATTAT GACAG) [35] were synthesized by Sangon Biotech (Shanghai, China). Ultrapure water was prepared using a Milli-Q system (Bedford, MA, USA).

2.2 Preparation of novel SERS tags

The novel SERS tags consisted of regrown GNRs co-mediated by aptamers and Raman reporters, prepared using one-pot synthesis as illustrated in **Fig. 1A**. The GNRs were prepared via CTAB-mediated seed growth, as previously described [31]. Meanwhile, the aptamers were heated to 90°C to open the secondary structure and then immediately put on ice to maintain the open chain structure. Then, 90 μL the prepared GNRs were incubated with 2.97 μL 100 μM prepared aptamers for 1 h, followed by addition of 1 μL 1 mM Raman reporters. The tag-1 and tag-2 were synthesized separately. Aptamers of *E. coli* O157:H7 and DTNB were used for tag-1 syntheses, while aptamers of *S. typhimurium* and MBA for tag-2 syntheses. After another 1 h incubation, 2.5 μL 40 mM HA solution (pH 5.0) as mild reducing agent, and 1 μL 1% (w/w) $HAuCl_4$ solution as the gold precursor, were added to the solution, which then was shaken vigorously for 1.5 h to obtain the novel SERS tags. The SERS tags were purified by

centrifugation at 5000 × *g* for 3 min to remove the supernatant and then re-suspended in ultrapure water.

2.3 Characterization of SERS tags

UV-vis spectra were recorded on a Shimadzu UV-1780 spectrometer. Transmission electron microscopy (TEM) (HITACHI HT7700, Japan) was used to characterize the morphology of the nanostructures. Energy-dispersive spectrometry (EDS) and high-resolution transmission electron microscopy (HRTEM) were conducted using a JEOL JEM-2100F microscope at an accelerating voltage of 200 kV to obtain images representing the microscopic surface structures and element distributions. SERS detection was performed on a DXR Raman microscope (JY H-800, HORIBA), equipped with a 633 nm excitation laser and a 10 × objective confocal microscope (2 μm spot diameter and 5 cm^{-1} spectral resolution). Samples were excited using 15-mW laser power and a slit width of 50 μm, with a total integration time of 10 s for each SERS spectrum. Five spots were chosen randomly for each sample measurement.

2.4 Separation and detection of bacteria

Fe_3O_4-antibody capture probes were prepared by conjugating monoclonal antibodies onto MNPs. Briefly, 30 μL 1 mg/mL streptavidin-modified MNPs with 150 nm diameters was incubated with 0.6 μL 1 mg/mL biotinylated antibody for 45 min at 15 rpm in a 1% BSA-soaked centrifuge tube, which conducted in a disc rotary mixer at room temperature (25 °C). The surplus antibodies were removed by magnetic separation and PBS washing twice, and the monoclonal antibody-modified MNPs were suspended in PBS.

E. coli O157:H7 and *S. typhimurium* were cultured in LB medium at 37°C for 12 h and then serially diluted 10-fold with sterile PBS buffer to final concentrations from 10^8 to 10^1 cfu/mL. Then two kinds of antibody-modified MNPs (30 μL) were added. The mixture was incubated for 45 min at 15 rpm to form MNPs-bacteria complexes. After capture, the MNPs-bacteria complexes were separated and washed twice with PBS under a magnetic field. Then, 180 μL prepared SERS tags (0.4 nM each of tag-1 and tag-2) were added, followed by another 45-min incubation at 15 rpm. The capture probe–pathogen–SERS tag sandwich complexes were collected and washed twice with PBS under a magnetic field and then used to measure the SERS spectra.

2.5 Optimization and evaluation of the established biosensor

The Raman signal intensity of the tags is a key performance factor of the biosensor and depends on the aptamers and Raman reporters. The concentrations of aptamer-1 and aptamer-2 (1.5, 2.0, 2.5, 3.0, 3.5, and 4.0 μM) and of DTNB and MBA (2.5, 5, 10, 20, 30, 40, and 50 μM) were tested to optimize the conditions for fabrication of tag-1 and tag-2. The various concentrations were evaluated according to the Raman signal intensity of the fabricated SERS tags to maximize the detection sensitivity. Then, we determined the optimum concentration of tags by adding various concentrations (0.1, 0.2, 0.3, 0.4, 0.5, and 0.6 nM) of tags into 10^6 cfu/mL pathogens.

Suspensions of *E. coli* O157:H7 and *S. typhimurium* at concentrations of 10^8–10^1 cfu/mL were used to determine the range of pathogen concentrations over which the biosensor response was linear. Partial least-squares (PLS) analyses were used to evaluate the linear relationship; the relationship was considered linear if the correlation coefficient, R, was close to 1, and the

root-mean-square error of calibration (RMSEC) was close to 0. The LOD was calculated according to the formula LOD = 3N/S, where N is the standard deviation of measurements on a blank sample and S is the slope of the standard curve. To evaluate the specificity of the biosensor, *E. coli*, *V. Parahemolyticus*, and *S. aureus* were used as interference bacteria. In addition, 20 random samples from a mixture of *E. coli* O157:H7 and *S. typhimurium* at 10^4 cfu/mL were selected to evaluate the reproducibility of the biosensor.

2.6 Analyses of food samples

Samples of tap water, cucumber, and chicken were used for realistic tests of the detection of *E. coli* O157:H7 and *S. typhimurium*. The samples were prepared according to previous reports with small modifications [14]. The food samples of cucumber and chicken were washed with ultrapure water and homogenized, filtered to remove solid precipitates, and then mixed with PBS at a ratio of 1: 9 (w/v). Then, *E. coli* O157:H7 and *S. typhimurium* at concentrations of 3.5×10^2 and 2.0×10^3 cfu/mL were added to each sample, respectively. After that, antibody-modified MNPs and SERS tags were added into spiked sample subsequently for separation and labelling according to Section 2.4. Finally, the Raman detection was conducted to calculate the concentration of bacteria. Traditional plate counting was also used to assess the recovery and accuracy of the Raman detection method. The recovery rate was calculated as the ratio of concentrations measured using SERS to the concentrations measured using the plate counting method. The accuracy was represented by relative standard deviation (RSD).

2.7 Data analyses

SERS spectra were recorded and analyzed using LabSpec application software and TQ analyst software (v8.0, Thermo Fisher Scientific). The raw SERS spectra were pre-processed by

smoothing the data and adjusting the baseline for later analyses. All the experiments were repeated three times. For each sample analyzed by SERS, five spots were selected randomly and scanned in the range of 400-2000 cm^{-1}.The results are presented as means and standard deviation, calculated using Origin 8.0.

3 Results and discussion

3.1 Design principles of the novel SERS biosensor for pathogens

The sensitive and simultaneous detection of *E. coli* O157:H7 and *S. typhimurium* were carried out based on two kinds of morphologically controllable, novel SERS tags, which exhibited strong Raman signals and bio-recognition specificities (**Fig. 1**). The SERS tag-1, which was synthesized using DTNB and an aptamer complementary to *E. coli* O157:H7, acquired a cracked octahedral shape, while the SERS tag-2, which was synthesized using MBA and an aptamer complementary to *S. typhimurium*, acquired small protrusions (**Fig. 1A**). Both aptamers and Raman reporters, when incubated with GNRs in the one-pot synthesis, successfully adsorbed onto the surfaces of the GNRs, which then grew into morphologically controllable tags. The cracked octahedral shape of tag-1 and the small protrusion morphology of tag-2 created more hotspots (localized regions of intense electromagnetic field enhancement), which greatly enhanced the Raman signal [31]. Meanwhile, the embedded Raman reporters in the outer layers of the SERS tags resulted in stable and strong Raman signal enhancements [17], which contributed to the sensitivity and overcame any signal interference arising from the simultaneous detection of multiple pathogens. During the regrowth process, the mononucleotide repeats at the 5’ ends of the aptamers stably anchored the SERS tags into the GNRs [29], comparable to thiol-modified aptamers. The aptamers not only tuned the regrowth process of the GNRs to a

programmed morphology, but also retained bio-recognition specificity for *E. coli* O157:H7 and *S. typhimurium*. The SERS tags specifically labeled the target pathogens to form sandwich complexes with antibody-modified MNPs, thereby realizing simultaneous SERS detection of the pathogens (**Fig. 1B**).

3.2 Characterization of the SERS tags

The SERS tags, being key factors for the performance of the biosensor, were characterized by UV–vis absorption spectroscopy, TEM, HRTEM, EDS, and SERS. The prepared GNRs displayed a blue-green color with transverse and longitudinal localized surface plasmon resonance (T-LSPR and L-LSPR) peaks at 516 and 650 nm, respectively. The colors for Tag-1 and Tag-2 changed to reddish purple and blueish purple, and the T-LSPR and L-LSPR peaks were red-shifted to 527 and 670 nm, and 538 and 677 nm, respectively (**Fig. 2A**). The red shift of the LSPR peaks and their separations suggest that the re-grown GNRs in the one-pot synthesis of the SERS tags were larger and more uniform in shape than the original GNRs. To investigate the shape of synthesized SERS tags, TEM was used to characterize the morphology of the SERS tags. The original GNRs had a well-defined rod shape and an average aspect ratio of 2.5 (width ~22 nm, length ~55 nm). The GNRs grown with DTNB and aptamer-1 exhibited a cracked octahedral shape with a smooth surface (tag-1), while the GNRs grown with MBA and aptamer-2 exhibited small protrusions and a rough surface (tag-2). The average aspect ratios of tag-1 and tag-2 were both about 2.0 (tag-1: width ~32 nm, length ~65 nm; tag-2: width ~40 nm, length ~80 nm). The TEM results confirmed the larger and more uniform morphologies of the GNRs in tag-1 and tag-2, in agreement with the red-shifted LSPR peaks. Differences in the UV-vis absorption spectra of tag-1 and tag-2 may reflect the distinct shapes and gap distances between pointed ends. Notably, the different morphologies of tag-1 and tag-2 may be attributed

to the sequence of nucleotides at the 5' ends of the aptamers. As previously reported, GNRs grown with homopolymeric thymine (T20) grew into cracked octahedral with smooth facets [31], as did our own tag-1. However, the GNRs in tag-2, which were grown with MBA and Aptamer-2, which contained homopolymeric cytosine (C20) at the 5' end, grew small protrusions and had a rough surface. Therefore, we speculated that the overgrowth time and concentrations of Raman reporters both have effect on the morphology of tags.

The successful fabrication of the SERS tags was further confirmed by HRTEM imaging and EDS. The magnified HRTEM images of the edges of tag-1 (**Fig. S1A** and **S1B**) and tag-2 (**Fig. S1C** and **S1D**) show that the aptamers were uniformly distributed around the SERS tags in a layer about 3.2 nm and 2.7 nm thick, respectively. The EDS image shows the presence of aptamer-1 (element P) and DTNB (element S) in cracked octahedral-shaped tag-1 (element Au, **Fig. 2B**) and the presence of aptamer-2 and MBA in small protrusion-shaped tag-2 (**Fig. 2C**), demonstrating the successful embedding of aptamers and Raman reporters in the gold shell of the SERS tags.

The SERS tags also exhibited greater enhancement effects, compared to the GNRs, presumably due to the adhered and embedded Raman reporters (**Fig. 2D** and **2E**). Raman enhancement factors (EFs) were 1.71×10^5 and 2.03×10^5 for tag-1 and tag-2, respectively, which were four times greater than the EFs for the Raman reporters adsorbed on the surface of GNRs without the aptamers. The Raman signal intensity depends largely on electromagnetic enhancement of the geometrically defined surface plasmon resonances of the nanomaterials. Here, the Raman signal enhancement was facilitated not just by the adhered and embedded Raman reporters, but also by the tuned, irregular shapes, which produced more Raman hotspots. These stronger EFs could facilitate the detection sensitivity of the biosensor.

3.3 Optimization of the SERS-based biosensor

During the one-pot synthesis of the SERS tags, the aptamers and Raman reporters compete for limited binding space on the growing GNRs [32]. Thus, the concentrations of aptamers and Raman reporters needed to be optimized to obtain the strongest possible Raman signal enhancement. With increasing concentrations of aptamer and Raman reporter, the Raman signal intensity of the SERS tags increased, reached an optimum, and then decreased (**Fig. 3A**-**3D**). To facilitate the sensitive and simultaneous detection of *E. coli* O157:H7 and *S. typhimurium*, the optimal concentrations of aptamer-1, aptamer-2, DTNB, and MBA for the one-pot syntheses of the SERS tags were 3.0, 2.5, 10.0, and 10.0 μM, respectively. To determine the optimal concentration of tags in the biosensor system, various concentrations of tag-1 and tag-2 were added separately into a 10^6 cfu/mL suspension of *E. coli* O157:H7 and *S. typhimurium*. The strongest characteristic Raman signal for sandwich complexes was obtained when the concentration of the added tag was 0.4 nm, for both tag-1 and tag-2 (**Fig. 3E** and **3F**, respectively). This result also demonstrated specific binding between the pathogens and the SERS tags.

The formation of capture probe–pathogen–SERS tag sandwich complexes were further indicated by TEM imaging. The cracked octahedral-shaped tag-1 was observed binding to *E. coli* O157:H7 (**Fig. 4A**), while the small protrusion-shaped tag-2 was observed binding to *S. typhimurium* (**Fig. 4B**). When both pathogens were present, tag-1 and tag-2 were each specifically bound to their respective pathogens: tag-1 to *E. coli* O157:H7 and tag-2 to *S. typhimurium* (**Fig. 4C**). The capture capability of the antibody-modified MNPs was confirmed by traditional plate counting. The capture rates for *E. coli* O157:H7 and *S. typhimurium* were above 90% in bacterial suspensions up to 10^6 cfu/mL (**Fig. 4D** and **4E**, respectively). The

stability and specificity of the capture probes contributed to the sensitive and simultaneous detection of the pathogens by the biosensor.

3.4 Evaluation of the analytical performance

The individual and simultaneous detection of *E. coli* O157:H7 and/or *S. typhimurium* were carried out under optimized conditions. For the individual detection, the favorable linear range of concentrations was first explored by detecting gradient concentrations (10^1 to 10^8 cfu/mL) of *E. coli* O157:H7 and *S. typhimurium*. Raman peaks of tag-1 at 1331 cm^{-1} and tag-2 at 1074 cm^{-1}, attributed to DTNB and MBA, respectively, were chosen for the quantitative analyses of *E. coli* O157:H7 and *S. typhimurium*. The Raman signal intensity grew rapidly with increasing concentrations of pathogens from 10^1 to 10^6 cfu/mL, and PLS analyses showed a good linear relationship (**Fig. S2**). There were strong linear correlations between the intensity of the Raman signal and the logarithms of the concentrations of *E. coli* O157:H7 ($y = 105.4x + 254.7$, $R^2 = 0.9942$) and *S. typhimurium* ($y = 87.6x + 59.5$, $R^2 = 0.9955$) with LOD values of 3 and 5 cfu/mL, respectively (**Fig. S3**). These results demonstrate that the biosensor was sensitive and quantitative for single-pathogen detection. For the simultaneous detection of *E. coli* O157:H7 and *S. typhimurium*, the characteristic peaks were readily separated, and both peak intensities gradually increased with increasing concentration of pathogens (**Fig. 5A**). There were still good linear correlations between 10^1 cfu/mL and 10^6 cfu/mL for *E. coli* O157:H7 ($y = 91.0x + 185.7$, $R^2 = 0.9914$) and *S. typhimurium* ($y = 64.2x + 99.7$, $R^2 = 0.9800$) with LOD values of 5 and 8 cfu/mL, respectively (**Fig. 5B**). The LOD values for *E. coli* O157:H7 and *S. typhimurium* were of the same order, indicating strong specificity for the tags and capture probes, with little signal interference between them. Compared to other SERS methods for the simultaneous detection of pathogens (**Table S1**) [36-38], the lower LOD values and wider linear range observed with our

297 biosensor confirmed its outstanding quantitative performance, which we attribute to the stable
298 and strong Raman signals of the novel SERS tags. With regard to localized surface plasmon
299 resonance (LSPR) method, bacteria could be monitored by measuring the wavelength shift in the
300 LSPR resonance peak, however, LOD values are relatively high [39, 40]. As for electrochemical
301 biosensors, the non-specific adsorption on the electrode affects the sensitivity and specificity of
302 detection [34]. In this study, the specific affinity of antibodies and aptamers enable high
303 detection specificity and sensitivity. In combination with specific shaped SERS tags, which
304 could provide strong characteristic Raman signals, the established biosensor could achieve more
305 sensitive detection for pathogens compared with the label-free method.

306 Good reproducibility was verified by taking 20 random samples from a mixed suspension of
307 *E. coli* O157:H7 and *S. typhimurium* at 10^4 cfu/mL. Their RSDs were 8.33% and 9.91%,
308 respectively (**Fig. 5C**). To verify the specificity of the biosensor, *E. coli*, *V. Parahemolyticus* and
309 *S. aureus* were used as interference bacteria. The signal intensities of *E. coli* O157:H7 and *S.*
310 *typhimurium* were almost 100-fold stronger than those of the non-target pathogens (**Fig. 5D**). A
311 very weak signal intensity in non-target samples (with MNPs but no tags) indicated that Raman
312 signals enhancement was contributed from SERS tags rather than MNPs. Furthermore, *E. coli*
313 O157:H7 and *S. typhimurium* were precisely detected in mixed samples, which consisted of *E.*
314 *coli* O157:H7, *S. typhimurium*, *E. coli*, *S. aureus*, and *Vibrio parahemolyticus*, attributed to the
315 high specific affinity of the tags and capture probes for their target pathogens. Good
316 reproducibility and specificity further demonstrate the reliability of our detection method.

317 To further investigate the applicability of the SERS biosensor for *E. coli* O157:H7 and
318 *S. typhimurium* in practical use, tap water, cucumber, and chicken were examined as models, and
319 our detection results were compared to the classic plate counting method as a standard [36]. As

shown in **Table 1**, the recovery rate for *E. coli* O157:H7 and *S. typhimurium* ranged from 95.92% to 105.32%, and 95.26% to 107.88%, respectively, indicating applicability and good accuracy of the proposed biosensor for the quantification of *E. coli* O157:H7 and *S. typhimurium* counts in food samples. "Plate counting" method needs at least 12 hours for culture, the SERS biosensor method established in this study was much faster (about 1 hour). Besides, the detection specificity can be guaranteed by the affinity of antibodies and aptamers, as well as the characteristic Raman signals produced by different SERS tags, while plate counting method needs further morphological identification. These results further demonstrate the bio-recognition specificity of the two novel SERS tags and the absence of signal interference during simultaneous SERS detection of pathogens.

4 Conclusions

The sensitive and simultaneous SERS detection of *E. coli* O157:H7 and *S. typhimurium* was achieved without signal interference by using a biosensor containing two kinds of aptamers and Raman reporters as novel SERS tags, which exhibit strong, stable Raman signals and bio-recognition capabilities. The cracked octahedral-shaped tag-1 and small protrusion-shaped tag-2 provided strong EFs of 1.71×10^5 and 2.03×10^5, respectively, which boosted detection sensitivity. The embedded Raman reporters and anchored aptamers with specific bio-recognition capacity made possible the avoidance of signal interference during the simultaneous detection of multiple pathogens. With monoclonal antibody-modified MNPs as capture probes, we were able to specifically separate and enrich the target pathogens, *E. coli* O157:H7 and *S. typhimurium*, demonstrating effective, sensitive and specific SERS detection of multiple pathogens. This biosensor had good quantitative capability between the Raman signal intensity and the

logarithms of the concentrations of *E. coli* O157:H7 and *S. typhimurium* from 10^1 to 10^6 cfu/mL in a suspension of multiple pathogens, with LOD values of 5 and 8 cfu/mL, respectively. The recovery rates from three spiked food samples ranged from 95.26% to 107.88%, demonstrating promising potential of the biosensor method to detect various pathogens, facilitating early screening of contaminated food. This biosensor, benefiting from the flexible combination of aptamers and Raman reporters in novel SERS tags, may possibly become a universal detection tool for the simultaneous detection of other foodborne pathogens.

Acknowledgments

The authors would like to acknowledge the financial support provided by National Natural Science Foundation of China (Nos. 31401581 and 31901776). We also appreciate the financial support from Agricultural Science Innovation Program (S2019XK02), Central Public-interest Scientific Institution Basal Research Fund (No. Y2019PT20-01), and Elite Youth Program of Chinese Academy of Agricultural Sciences.

Declaration of Competing Interest

The authors declare no competing financial interest.

Appendix A. Supplementary data

Supplementary data associated with this article can be found in the online version. High-resolution TEM images of SERS tags-1 and tags-2 (**Fig. S1**); Partial least-squares (PLS) analyses of *E. coli.* O157: H7 and *S. typhimurium* concentration prediction (**Fig. S2**); Linear correlation between the logarithm of pathogen concentrations and SERS intensity for *E. coli.*

O157: H7 and *S. typhimurium* in single detection system (**Fig. S3**); Comparison of various methods for the simultaneous detection of pathogens by SERS (**Table S1**).

References

[1] T. Jiang, Y. Song, T. Wei, H. Li, D. Du, M. Zhu, et al., Sensitive detection of *Escherichia coli* O157:H7 using Pt-Au bimetal nanoparticles with peroxidase-like amplification, Biosens. Bioelectron. 77 (2016) 687−694, https://doi.org/10.1016/j.bios.2015.10.017.

[2] M.M.A. Zeinhom, Y. Wang, Y. Song, M. Zhu, Y. Lin, D. Du, A portable smart-phone device for rapid and sensitive detection of *E. coli* O157:H7 in Yoghurt and Egg, Biosens. Bioelectron. 99 (2018) 479−485, https://doi.org/10.1016/j.bios.2017.08.002.

[3] M.E. Arnold, J.J. Carrique-Mas, I. McLaren, R.H. Davies, A comparison of pooled and individual bird sampling for detection of *Salmonella* in commercial egg laying flocks, Prev. Vet. Med. 99 (2011) 176−184, https://doi.org/10.1016/j.prevetmed.2010.12.007.

[4] H. Can, T.H. Celik, Detection of enterotoxigenic and antimicrobial resistant *S. aureus* in Turkish cheeses, Food Control 24 (2012) 100−103, https://doi.org/10.1016/j.foodcont.2011.09.009.

[5] X. Zhao, C. Lin, J. Wang, D.H. Oh, Advances in rapid detection methods for foodborne pathogens, J. Microbiol. Biotechnol. 24 (2014) 297−312, https://doi.org/10.4014/jmb.1310.10013.

[6] F. Yeni, S. Acar, Ö.G. Polat, Y. Soyer, H. Alpas, Rapid and standardized methods for detection of foodborne pathogens and mycotoxins on fresh produce, Food Control 40 (2014) 359−367, https://doi.org/10.1016/j.foodcont.2013.12.020.

[7] F. Min, Q. Yong, W. Wang, K. Hua, L. Wang, C. Xu, Development of a monoclonal antibody-based ELISA to detect *Escherichia coli* O157:H7, Food Agric. Immunol. 24 (2013) 481−487, https://doi.org/10.1080/09540105.2012.716026.

[8] M. Safavieh, M.U. Ahmed, M. Tolba, M. Zourob, Microfluidic electrochemical assay for rapid detection and quantification of *Escherichia coli*, Biosens. Bioelectron. 31 (2012) 523−528, https://doi.org/10.1016/j.bios.2011.11.032.

[9] X. Su, Y. Li, A QCM immunosensor for *Salmonella* detection with simultaneous measurements of resonant frequency and motional resistance, Biosens. Bioelectron. 21 (2005) 840−848, https://doi.org/10.1016/j.bios.2005.01.021.

[10] N. Karoonuthaisiri, R. Charlermroj, M.J. Morton, M. Oplatowska-Stachowiak, I.R. Grant, C.T. Elliott, Development of a M13 bacteriophage-based SPR detection using *Salmonella* as a case study, Sens. Actuators, B 190 (2014) 214−220, https://doi.org/10.1016/j.snb.2013.08.068.

[11] J. Chen, S.M. Andler, J.M. Goddard, S.R. Nugen, V.M. Rotello, Integrating recognition elements with nanomaterials for bacteria sensing, Chem. Soc. Rev. 46 (2017) 1272−1283, https://doi.org/10.1039/c6cs00313c.

[12] Y. Liu, H. Zhou, Z. Hu, G. Yu, D. Yang, J. Zhao, Label and label-free based surface-enhanced Raman scattering for pathogen bacteria detection: A review, Biosens. Bioelectron. 94 (2017) 131−140, https://doi.org/10.1016/j.bios.2017.02.032.

[13] C. Zhang, C. Wang, R. Xiao, L. Tang, J. Huang, D. Wu, et al., Sensitive and specific detection of clinical bacteria via vancomycin-modified Fe_3O_4@Au nanoparticles and aptamer-functionalized SERS tags, J. Mater. Chem. B 6 (2018) 3751−3761, https://doi.org/10.1039/c8tb00504d.

[14] H. Zhang, X. Ma, Y. Liu, N. Duan, S. Wu, Z. Wang, et al., Gold nanoparticles enhanced SERS aptasensor for the simultaneous detection of *Salmonella typhimurium* and

Staphylococcus aureus, Biosens. Bioelectron. 74 (2015) 872−877, https://doi.org/10.1016/j.bios.2015.07.033.

[15] L. Lin, Q. Zhang, X. Li, M. Qiu, X. Jiang, W. Jin, et al., Electron transport across plasmonic molecular nanogaps interrogated with surface-enhanced Raman scattering, Acs Nano 12 (2018) 6492−6503, https://doi.org/10.1021/acsnano.7b08224.

[16] D. Graham, M. Moskovits, Z.Q. Tian, SERS - facts, figures and the future, Chem. Soc. Rev. 46 (2017) 3864−3865, https://doi.org/10.1039/c7cs90060k.

[17] M. Li, J. Zhang, S. Suri, L.J. Sooter, D. Ma, N. Wu, Detection of adenosine triphosphate with an aptamer biosensor based on surface-enhanced Raman scattering, Anal. Chem. 84 (2012) 2837−2842, https://doi.org/10.1021/ac203325z.

[18] Y. Zhao, J. Zhao, G. Shan, D. Yan, Y. Chen, Y. Liu, SERS-active liposome@Ag/Au nanocomposite for NIR light-driven drug release, Colloids surf., B 154 (2017) 150−159, https://doi.org/10.1016/j.colsurfb.2017.03.016.

[19] Q. Zhang, X. Lu, P. Tang, D. Zhang, J. Tian, L. Zhong, Gold nanoparticle (AuNP)-based surface-enhanced Raman scattering (SERS) probe of Leukemic Lymphocytes, Plasmonics 11 (2016) 1361−1368, https://doi.org/10.1007/s11468-016-0185-6.

[20] Y. Wang, B. Yan, L. Chen, SERS tags: novel optical nanoprobes for bioanalysis, Chem. Rev. 113 (2013) 1391−1428, https://doi.org/10.1021/cr300120g.

[21] B. Williamson, Jr., R.R. Hattery, D.H. Stephens, P.F. Sheedy, 2nd, Computed tomography of the kidneys, Semin. Roentgenol. 13 (1978) 249−255, https://doi.org/10.1007/s00604-017-2298-9.

[22] T. Le, P. Chang, D. Benton, J.W. Mccauley, M. Iqbal, C. Aeg, Dual recognition element lateral flow assay (DRELFA)- towards multiplex strain specific influenza virus detection, Anal. Chem. 89 (2017) 6781−6786, https://doi.org/10.1021/acs.analchem.7b01149.

[23] K. Kim, H.B. Lee, Y.M. Lee, K.S. Shin, Rhodamine B isothiocyanate-modified Ag nanoaggregates on dielectric beads: a novel surface-enhanced Raman scattering and fluorescent imaging material, Biosens. Bioelectron. 24 (2009) 1864−1869, https://doi.org/10.1016/j.bios.2008.09.017.

[24] L. Guerrini, D. Graham, Molecularly-mediated assemblies of plasmonic nanoparticles for surface-enhanced Raman spectroscopy applications, Chem. Soc. Rev. 41 (2012) 7085−7107, https://doi.org/10.1039/c2cs35118h.

[25] J.H. Lee, G.H. Kim, J.M. Nam, Directional synthesis and assembly of bimetallic nanosnowmen with DNA, J. Am. Chem. Soc. 134 (2012) 5456−5459, https://doi.org/10.1021/ja2121525

[26] J.W. Oh, D.K. Lim, G.H. Kim, Y.D. Suh, J.M. Nam, Thiolated DNA-based chemistry and control in the structure and optical properties of plasmonic nanoparticles with ultrasmall interior nanogap, J. Am. Chem. Soc. 136 (2014) 14052−14059, https://doi.org/10.1021/ja504270d.

[27] J. Shen, L. Xu, C. Wang, H. Pei, R. Tai, S. Song, et al., Dynamic and quantitative control of the DNA-mediated growth of gold plasmonic nanostructures, Angew. Chem., Int. Ed. 53 (2014) 8338−8342, https://doi.org/10.1002/anie.201402937.

[28] L.M. Demers, M. Ostblom, H. Zhang, N.H. Jang, B. Liedberg, C.A. Mirkin, Thermal desorption behavior and binding properties of DNA bases and nucleosides on gold, J. Am. Chem. Soc. 124 (2002) 11248−11249, https://doi.org/10.1021/ja0265355.

[29] T. Song, L. Tang, L. Tan, X. Wang, N.S. Satyavolu, H. Xing, et al., DNA-encoded tuning of geometric and plasmonic properties of nanoparticles growing from gold nanorod seeds, Angew. Chem., Int. Ed. 54 (2015) 8114−8118, https://doi.org/10.1002/anie.201500838.

[30] Z. Wang, L. Tang, L.H. Tan, J. Li, Y. Lu, Discovery of the DNA "Genetic Code" for abiological gold nanoparticle morphologies, Angew. Chem., Int. Ed. 51 (2012) 9078−9082, https://doi.org/10.1002/anie.

[31] J. Li, J. Zhou, T. Jiang, B. Wang, M. Gu, L. Petti, et al., Controllable synthesis and SERS characteristics of hollow sea-urchin gold nanoparticles, Phys. Chem. Chem. Phys. 16 (2014) 25601−25608, https://doi.org/10.1039/c4cp04017a.

[32] Y. Li, X. Liu, D. Jiang, Z. Yu, D. Tian, C. Lu, et al., One-pot synthesis of a DNA-anchored SERS nanoprobe with simultaneous nanostructural tuning and Raman reporter encoding, Rsc. Adv. 7 (2017) 5063−5066, https://doi.org/10.1039/c6ra26580d.

[33] S. Zhou, C. Lu, Y. Li, L. Xue, C. Zhao, G. Tian, et al., Gold nanobones enhanced ultrasensitive surface-enhanced Raman scattering aptasensor for detecting *Escherichia coli* O157:H7. ACS Sens. (2020), https://doi.org/10.1021/acssensors.9b02600.

[34] L. Yao, L. Wang, F. Huang, G. Cai, X. Xi, J. Lin, A microfluidic impedance biosensor based on immunomagnetic separation and urease catalysis for continuous-flow detection of *E. coli* O157:H7, Sens. Actuators, B 259 (2018) 1013−1021, https://doi.org/10.1016/j.snb.2017.12.110.

[35] R. Joshi, H. Janagama, H.P. Dwivedi, T.M. Senthil Kumar, L.A. Jaykus, J. Schefers, et al., Selection, characterization, and application of DNA aptamers for the capture and detection of *Salmonella enterica serovars*, Mol. Cell. Probes 23 (2009) 20−28, https://doi.org/10.1016/j.mcp.2008.10.006.

[36] Y. Wang, S. Ravindranath, J. Irudayaraj, Separation and detection of multiple pathogens in a food matrix by magnetic SERS nanoprobes, Anal. Bioanal. Chem. 399 (2011) 1271−1278, https://doi.org/10.1007/s00216-010-4453-6.

[37] S.P. Ravindranath, Y. Wang, J. Irudayaraj, SERS driven cross-platform based multiplex pathogen detection, Sens. Actuators, B 152 (2011) 183−190, https://doi.org/10.1016/j.snb.2010.12.005.

[38] K. Yuan, Q. Mei, X. Guo, Y. Xu, D. Yang, B.J. Sanchez, et al., Antimicrobial peptide based magnetic recognition elements and Au@Ag-GO SERS tags with stable internal standards: a three in one biosensor for isolation, discrimination and killing of multiple bacteria in whole blood, Chem. Sci. 9 (2018) 8781−8795, https://doi.org/10.1039/c8sc04637a.

[39] N. Formisanoa, N. Bhallaa, M. Heeranb, J.R. Martinezb, A. Sarkarb, M. Laabeic, et al., Inexpensive and fast pathogenic bacteria screening using field-effect transistors, Biosens. Bioelectron. 85 (2016) 103−109, https://doi.org/10.1016/j.bios.2016.04.063.

[40] N.R. Funari, N. Bhalla, K.Y. Chu, B. Söderström, A.Q. Shen, Nanoplasmonics for real-time and label-free monitoring of microbial biofilm formation, ACS Sens. 3 (2018) 1499−1509, https://doi.org/10.1021/acssensors.8b00287.

Captions

Fig. 1 Schematic illustration of the SERS detection biosensor. Principles of the one-pot synthesis of SERS tags co-mediated with aptamers and Raman reporters (A), and the separation and SERS detection of *E. coli* O157:H7 and *S. typhimurium* (B).

Fig. 2 Characterization of the SERS tags. UV absorption spectra, appearance, and transmission electron microscopy (TEM) images of GNRs and SERS tags (A); high-resolution TEM (HR TEM) images and energy dispersive spectrometer images of tag-1 (B) and tag-2 (C): P = aptamer, S = Raman reporter, Au = gold nanorod; Raman enhancement of tag-1 (D) and tag-2 (E).

Fig. 3 Optimization of the SERS biosensor. Effects of aptamer-1 concentration on tag-1 (A), aptamer-2 concentration on tag-2 (B), concentration of 5,5'-dithiobis-(2-nitrobenzoic acid) on tag-1 (C), concentration of 4-mercaptobenzoic acid on tag-2 (D), tag-1 concentration on *E. coli O157:H7* detection (E), and tag-2 concentration on *S. typhimurium* detection (F).

Fig. 4 Bio-recognition specificity of the capture probes and SERS tags. TEM image of the capture probe–pathogen–SERS tag sandwich complexes and corresponding magnified image, obtained from the square area, of *E. coli O157:H7* (A), *S. typhimurium* (B), and the mixture of *E. coli O157:H7* and *S. typhimurium* (C); capture rates of the capture probes at different concentrations of *E. coli*. *O157: H7* (D) and *S. typhimurium* (E).

Fig. 5 Evaluation of quantitative detection, signal stability and specificity properties of the SERS biosensor. (A) SERS spectrum for *E. coli*. *O157: H7* and *S. typhimurium* in a mixed system; (B) Linear correlation between the logarithms of pathogen concentrations and SERS intensities of the peaks at 1330 cm^{-1} for *E. coli*. *O157: H7* and 1074 cm^{-1} for *S.*

typhimurium; (C) Raman intensities of 20 random samples separately measured from a suspension of *Escherichia coli*. O157: H7 and *Salmonella typhimurium* at 10^4 cfu/mL; (D) Raman intensities for *E. coli* O157:H7, *S. typhimurium* and three interfering bacteria. The mixture sample in Fig. 5D consisted of 5 different bacteria, including *E. coli* O157:H7, *S. typhimurium*, *E. coli*, *S. aureus*, and *Vibrio parahemolyticus*.

Table 1 Comparison of the simultaneous detection of *Escherichia coli* O157:H7 and *Salmonella typhimurium* in three real samples by the surface-enhanced Raman scattering biosensor, versus classic plate counting.

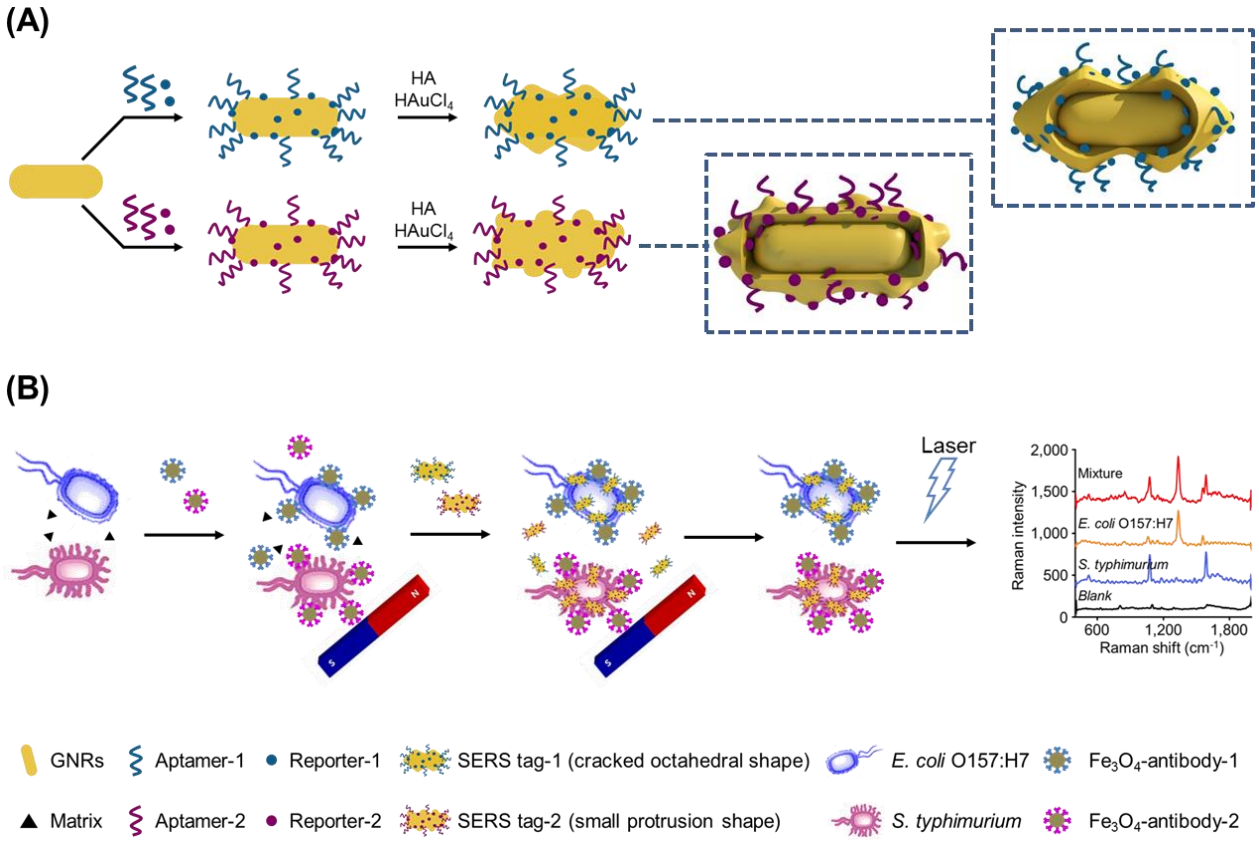
(A)
HA
HAuCl4
HA
HAuCl4
(B)
Laser
Raman intensity
2,000
1,500
1,000
500
0
Mixture
E. coli O157:H7
S. typhimurium
Blank
600
1,200
1,800
Raman shift (cm-1)
GNRs
Aptamer-1
Reporter-1
SERS tag-1 (cracked octahedral shape)
E. coli O157:H7
Fe3O4-antibody-1
Matrix
Aptamer-2
Reporter-2
SERS tag-2 (small protrusion shape)
S. typhimurium
Fe3O4-antibody-2

522

523 **Fig. 1**

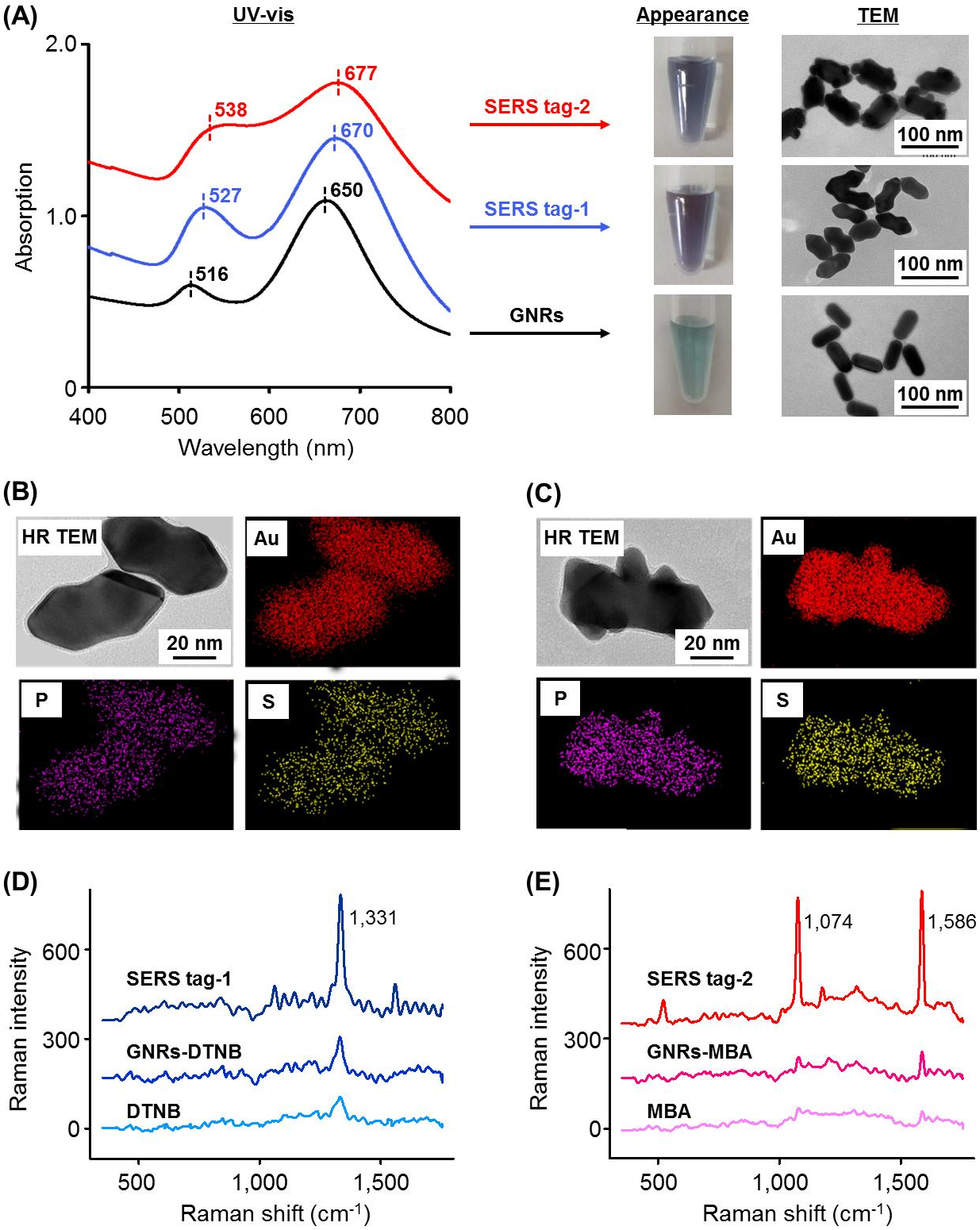
(A)
UV-vis
Appearance
TEM
2.0
1.0
0
Absorption
400
500
600
700
800
Wavelength (nm)
677
538
670
527
650
516
SERS tag-2
SERS tag-1
GNRs
100 nm
100 nm
100 nm
(B)
HR TEM
20 nm
Au
P
S
(C)
HR TEM
20 nm
Au
P
S
(D)
Raman intensity
600
300
0
1,331
SERS tag-1
GNRs-DTNB
DTNB
500
1,000
1,500
Raman shift (cm-1)
(E)
Raman intensity
600
300
0
1,074
1,586
SERS tag-2
GNRs-MBA
MBA
500
1,000
1,500
Raman shift (cm-1)

Fig. 2

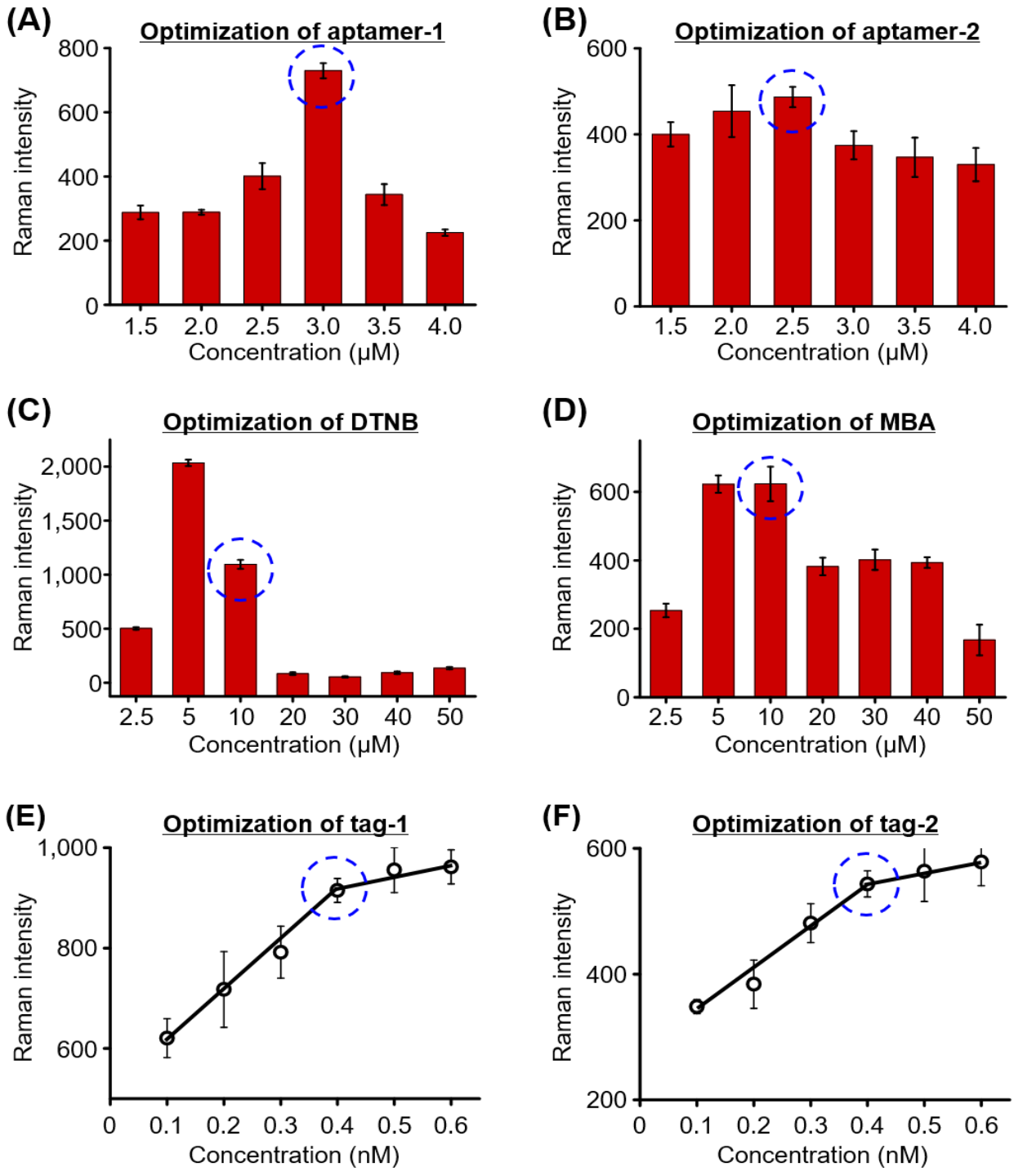
(A)
Optimization of aptamer-1
Raman intensity
800
600
400
200
0
1.5
2.0
2.5
3.0
3.5
4.0
Concentration (μM)
(B)
Optimization of aptamer-2
Raman intensity
600
400
200
0
1.5
2.0
2.5
3.0
3.5
4.0
Concentration (μM)
(C)
Optimization of DTNB
Raman intensity
2,000
1,500
1,000
500
0
2.5
5
10
20
30
40
50
Concentration (μM)
(D)
Optimization of MBA
Raman intensity
600
400
200
0
2.5
5
10
20
30
40
50
Concentration (μM)
(E)
Optimization of tag-1
Raman intensity
1,000
800
600
0
0.1
0.2
0.3
0.4
0.5
0.6
Concentration (nM)
(F)
Optimization of tag-2
Raman intensity
600
400
200
0
0.1
0.2
0.3
0.4
0.5
0.6
Concentration (nM)

526

527 **Fig. 3**

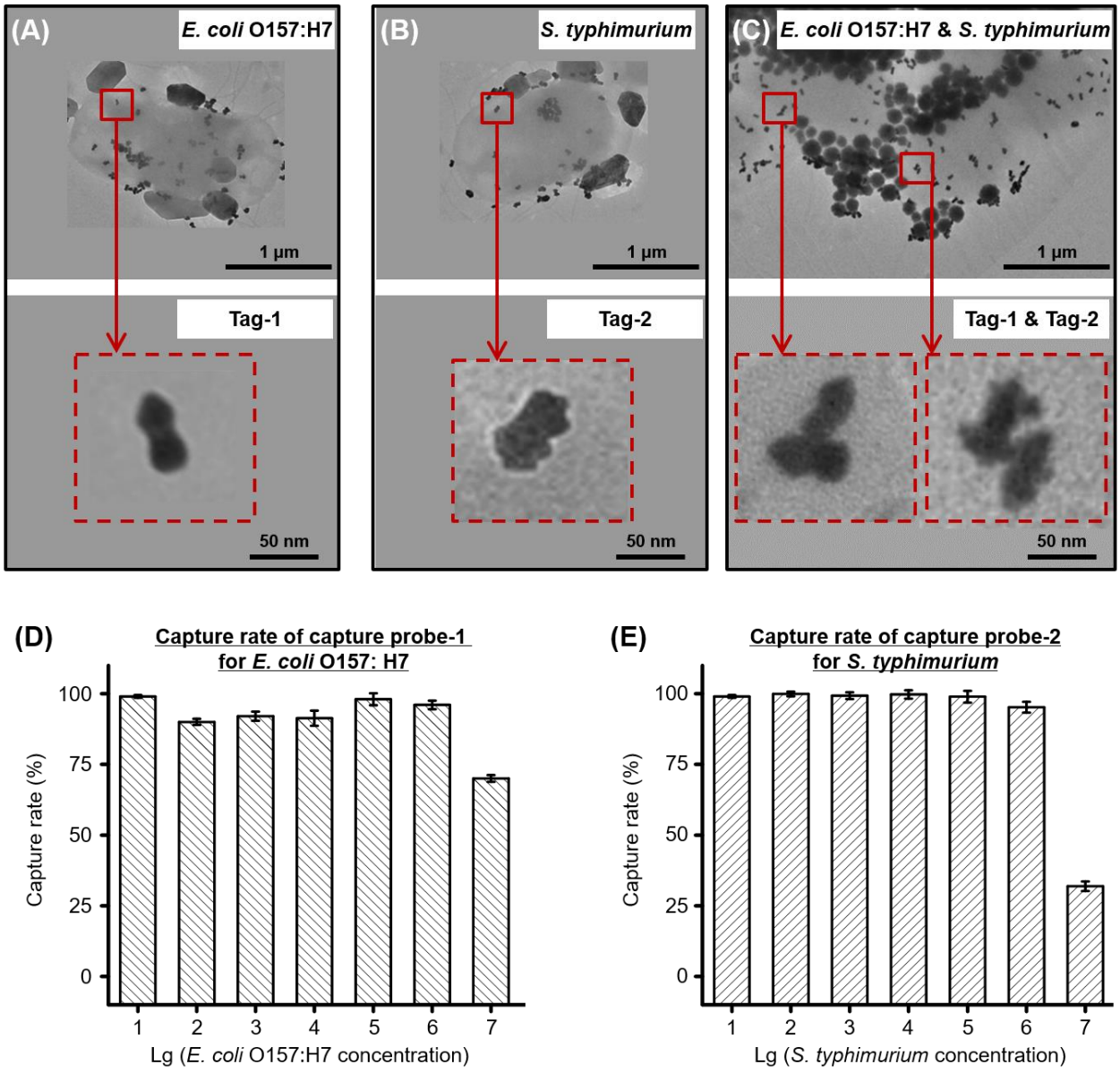
(A)
E. coli O157:H7
1 μm
Tag-1
50 nm
(B)
S. typhimurium
1 μm
Tag-2
50 nm
(C)
E. coli O157:H7 & S. typhimurium
1 μm
Tag-1 & Tag-2
50 nm
(D)
Capture rate of capture probe-1 for E. coli O157: H7
Capture rate (%)
Lg (E. coli O157:H7 concentration)
(E)
Capture rate of capture probe-2 for S. typhimurium
Capture rate (%)
Lg (S. typhimurium concentration)

528

529 **Fig. 4**

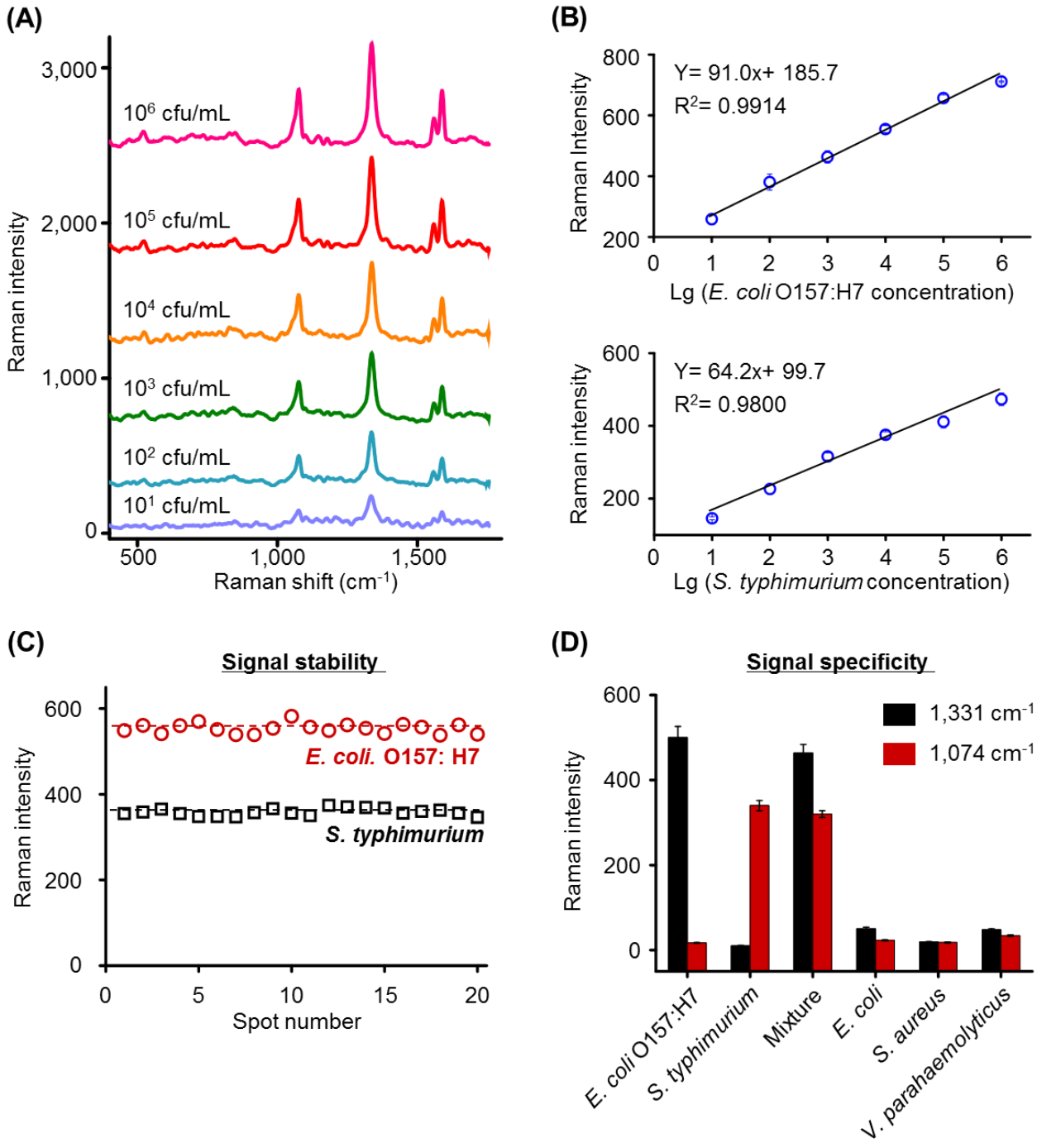
(A)
3,000
2,000
1,000
0
Raman intensity
10^6 cfu/mL
10^5 cfu/mL
10^4 cfu/mL
10^3 cfu/mL
10^2 cfu/mL
10^1 cfu/mL
500
1,000
1,500
Raman shift (cm^-1)
(B)
800
600
400
200
Raman Intensity
Y= 91.0x+ 185.7
R^2= 0.9914
0 1 2 3 4 5 6
Lg (E. coli O157:H7 concentration)
600
400
200
Raman intensity
Y= 64.2x+ 99.7
R^2= 0.9800
0 1 2 3 4 5 6
Lg (S. typhimurium concentration)
(C)
Signal stability
600
400
200
0
Raman intensity
E. coli. O157: H7
S. typhimurium
0 5 10 15 20
Spot number
(D)
Signal specificity
600
400
200
0
Raman intensity
1,331 cm^-1
1,074 cm^-1
E. coli O157:H7
S. typhimurium
Mixture
E. coli
S. aureus
V. parahaemolyticus

530

531 **Fig. 5.**

532 **Table 1**

	Our method		Plate counting method		Recovery rate (%)	
	***E. coli* O157:H7 (cfu/mL)**	***S. typhimurium* (cfu/mL)**	***E. coli* O157:H7 (cfu/mL)**	***S. typhimurium* (cfu/mL)**	***E. coli* O157:H7**	***S. typhimurium***
Tap water	329 ± 26	194 ± 13	343 ± 12	193 ± 8	95.92	100.52
Cucumber	357 ± 21	181 ± 15	367 ± 5	190 ± 8	97.28	95.26
Chicken	376 ± 32	219 ± 17	357 ± 16	203 ± 10	105.32	107.88

533